Redox-driven Conformational Dynamics in a Photosystem-II-inspired β-hairpin Maquette Determined through Spectroscopy and Simulation

Hyea Hwang[†,1], Tyler G. McCaslin[†,2,3] Anthony Hazel[4], Cynthia V. Pagba[2,3] Christina M. Nevin[2,3], Anna Pavlova[4], Bridgette A. Barry[2,3] and James C. Gumbart[2,3,4,*]

[1]School of Materials Science and Engineering, [2]School of Chemistry and Biochemistry, [3]Petit Institute for Bioengineering and Biosciences, and [4]School of Physics, Georgia Institute of Technology, Atlanta, GA 30332

† These authors contributed equally to this work.

* To whom correspondence should be addressed; Email: gumbart@physics.gatech.edu; Phone: 404-385-0797

Abstract

Tyrosine-based radical transfer plays an important role in photosynthesis, respiration, and DNA synthesis. Radical transfer can occur either by electron transfer (ET) or proton coupled electron transfer (PCET), depending on the pH. Reversible conformational changes in the surrounding protein matrix may control reactivity of radical intermediates. De novo designed Peptide A is a synthetic 18 amino-acid β-hairpin, which contains a single tyrosine (Y5) and carries out a kinetically significant PCET reaction between Y5 and a cross-strand histidine (H14). In Peptide A, amide II' (CN) changes are observed in the UV resonance Raman (UVRR) spectrum, associated with tyrosine ET and PCET; these bands were attributed previously to a reversible change in secondary structure. Here, we use molecular dynamics simulations to define this conformational change in Peptide A and its H14-to-cyclohexylalanine variant, Peptide C. Three different Y5 charge states, tyrosine (YH), tyrosinate (Y^-), and neutral tyrosyl radical (Y•), are considered. The simulations show that Peptide A-YH and A-Y^- retain secondary structure and noncovalent interactions, whereas A-Y• is unstable. In contrast, both Peptide C-Y^- and Peptide C-Y• are unstable, due to the loss of the Y5-H14 π-π interaction. These simulations are consistent with previous UVRR experimental results on the two β-hairpins. Furthermore, they demonstrate the ability of simulations using fixed-charge force fields to accurately capture redox-linked conformational dynamics in a β-strand peptide.

Introduction

Photosynthesis, respiration, and DNA synthesis involve essential electron transfer (ET) reactions. When these reactions operate at high potential, aromatic amino acids can play important roles in the mechanism. Redox-active tyrosine residues are known to be catalytically important in cytochrome c oxidase,[1-2] ribonucleotide reductase (RNR),[3] photosystem II (PSII),[4-5] and other enzymes such as prostaglandin H synthase,[6] galactose oxidase,[7] glyoxyl oxidase,[8] and *Mycobacterium tuberculosis* catalase-peroxidase.[9] Tyrosine side chains can participate in ET reactions either by tunneling or by hopping (multistep tunneling) mechanisms (reviewed in Ref. [10-12]). For outer sphere reactions, Marcus ET theory [13] predicts the dependence of the electron transfer rate (k_{ET}) on temperature (T), driving force (ΔG^o), nuclear reorganization energy (λ), and the electronic coupling (H_{AB}) between the reactants and products.

The pK_a of the tyrosine phenolic group is approximately 10,[14] while the pK_a of the phenolic group is below zero after oxidation of tyrosine.[15] Therefore, oxidation of tyrosine forms a neutral radical both at low and high pH. When the pH is above the pK_a of tyrosine (>10, Fig. 1), oxidation of tyrosine proceeds by an ET reaction.[16] When the pH is below the pK_a, (<10, Fig. 1), oxidation occurs via a proton coupled electron transfer (PCET) reaction, yielding both an electron and a proton. The PCET reaction can occur by three distinct mechanisms, proton first (PTET), electron first (ETPT), or a coupled movement of proton and electron (CPET) through the same transition state. The factors that control PCET reactions have been the focus of theory and experiment in a wide variety of model systems and proteins.[10-12, 17]

In the investigation of ET and PCET mechanisms, peptides provide simple, water soluble scaffolds. The use of unnatural amino acids in these scaffolds opens up new avenues for chemistry. The construction and study of such peptide models or maquettes has provideed valuable insight into biological reactions (for previous examples, see Refs. [18-30]).

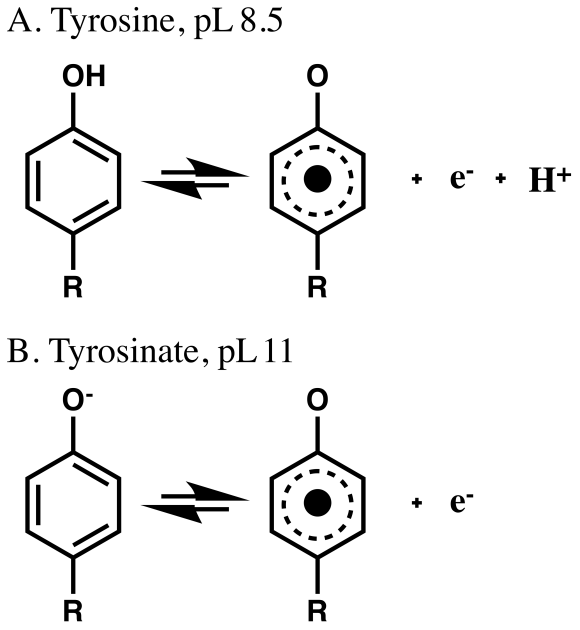

Figure 1. (A) Tyrosine and its PCET reaction to form a neutral tyrosyl radical and (B) tyrosinate and its ET reaction to form a neutral tyrosyl radical. The reaction in (A) occurs at pL 8.5; the reaction in (B) occurs at pL 11 (L is the lyonium ion).

To model tyrosine-based PCET in a β-hairpin, an 18-amino-acid sequence, Peptide A (Fig. 2C), which contains a single tyrosine (Y5) and a histidine (H14),[25, 27] was synthesized and characterized. The NMR structure of the peptide was determined, and it was shown that the peptide folds to form a β-hairpin. The Y5 and H14 are π-π stacked but not hydrogen bonded in the averaged, minimized structure.[31] Electrochemical data are consistent with a PCET reaction between histidine and tyrosine, when the tyrosyl radical is generated in the mid-pH range from singlet tyrosine. Oxidation of tyrosine results in a change in histidine pK_a, which leads to a proton transfer to the imidazole side chain. This reaction has been shown to be kinetically important in time-resolved absorption measurements on the picosecond time scale.[32-33] Interestingly, UV resonance Raman (UVRR) studies of Peptide A, which maintains the oxidized state for orders of magnitude greater time scales, have suggested that the tyrosine PCET/ET

reaction is accompanied by a reversible conformational change, attributed to a loss of β-strand interactions.[34] While the change could be observed in Peptide A either at pD 8.5 or 11, in a variant of Peptide A, in which H14 is replaced with cyclohexylalanine (Cha14, Peptide C, Fig. 2D), the amide II' bands were only detected at the lower pD value. Previous CD studies showed that both peptides experienced a reversible thermal transition at low and high pH values.[25, 27]

The potential contribution of protein motions in ET and PCET reactions has been discussed extensively.[11, 17, 35-38] Here, we investigate those motions using molecular dynamic simulations. In the simulations, we observed redox-induced conformational changes in two β-hairpin maquettes, Peptide A and Peptide C, which rationalize experimental spectroscopic data.

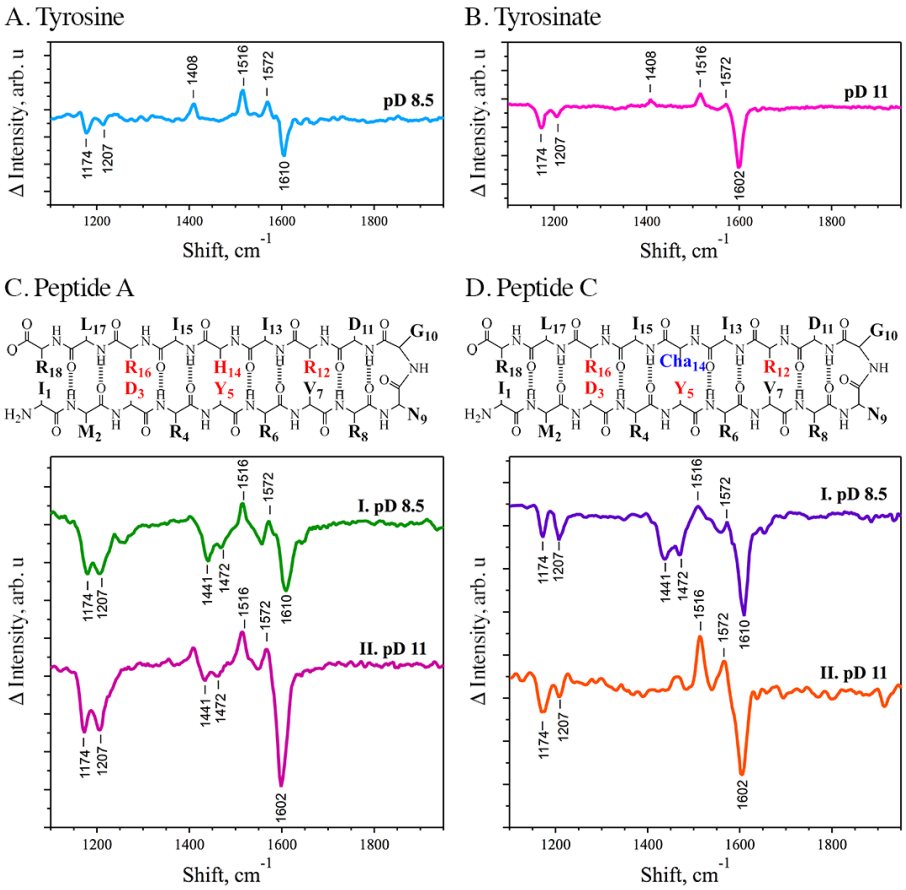

Figure 2: UVRR difference spectra, primary sequences, and predicted secondary structures. UVRR difference spectra (radical-minus-singlet) acquired from (A) tyrosine, pL 8.5 or (B) tyrosinate, pL 11 solution (L is the lyonium ion). Sequences and predicted fold of Peptide A (C) and its His14 to Cha14 variant, Peptide C (D). UVRR difference spectra (radical-minus-singlet) acquired from (C) Peptide A-YH at pD 8.5 (I) or Peptide A-Y^- at pD 11 (II) and from (D) Peptide C-YH at pD 8.5 (I) or Peptide C-Y^- at pD 11 (II). The difference spectra were calculated as radical-minus-singlet. A 244 nm Raman probe beam was utilized. The data are reproduced from Ref. [34].

Methods

Molecular dynamics simulations

The three-dimensional, averaged, and minimized structure of Peptide A (sequence IMDRYRVRNGDRIHIRLR), determined by NMR spectroscopy[31], was used as an initial structure. In Peptide A, H14 is singly protonated at the epsilon nitrogen. Because this histidine has an estimated pKa of 7.0 when Y5 is in a reduced state and 8.0 when Y5 is in an oxidized, radical state[25], roughly 3% of His14 in Peptide A-YH and 25% of His14 in Peptide A-Y• are doubly protonated at pD 8.5 in the UVRR experiments. Therefore, we also built a system in which H14 is doubly protonated.

Peptide C was built by replacing H14 with cyclohexylalanine (Cha14). For each variant, three different conditions were simulated to observe the conformational change and stability depending on the charge state of Y5. We denote these charge states Peptide A/C-YH (tyrosine), Peptide A/C-Y^- (charged tyrosine, tyrosinate), and Peptide A/C-Y• (neutral tyrosyl radical) based on the charge state of Y5 (see Fig. 1).

Because parameters for the tyrosyl radical are not present in the CHARMM protein force field, we optimized the partial atomic charges for this residue using the Force Field Toolkit in

VMD.[39-40] A reduced model for the side chain, truncated at CG (see Fig. 3), was used. We fitted the interaction energies with water molecules in molecular dynamics to those in quantum chemical calculations, as is standard in the CHARMM force field.[41] Because the restricted open-shell approach was shown to be more accurate than the unrestricted one for phenoxyl radical calculations with MP2 and HF methods,[42] this approach was used for geometry optimization of the radical state and for determining the interaction energies with water molecules. The geometry was optimized at the ROMP2(6-31G*) level of theory and the interaction energies with water molecules were calculated at the ROHF(6-31G*) level of theory. Gaussian09 was used for all QM calculations.[43] Only the charges of the phenol group were modified; the resulting MM interaction energies with water were within 0.2 kcal/mol of the target QM energies, as recommended for CHARMM parameters.[41] The resulting charges for Y•, shown in Table 1 and Fig. 3, produce an electrostatic potential qualitatively similar to one previously determined based on hybrid-functional calculations using B3LYP/6-311++G.[25]

All peptide models were solvated with TIP3P water and ions to neutralize the system in 100 mM NaCl. The initial size of the periodic box was 55×55×51 Å, providing 20-30 Å between periodic images of the protein in all three directions. Each system was minimized for 1000 steps, and the solvent was equilibrated while the peptide backbone was restrained for 2 ns. All analysis was done on 200-ns unrestrained production runs. Molecular dynamics simulations were carried out with NAMD[44] using the CHARMM36 force field.[45] A 2-fs time step was used. Bonded and short-range non-bonded interactions were calculated every time step, while long-range electrostatics were calculated every other time step using the particle-mesh Ewald (PME) method.[46] The long-range cutoff was set to 12 Å with a potential based switching function starting at 10 Å. The temperature was maintained at 300 K using Langevin dynamics, and the pressure was kept constant at 1 atm using the Langevin piston method. System setup and analysis were performed in VMD.[40]

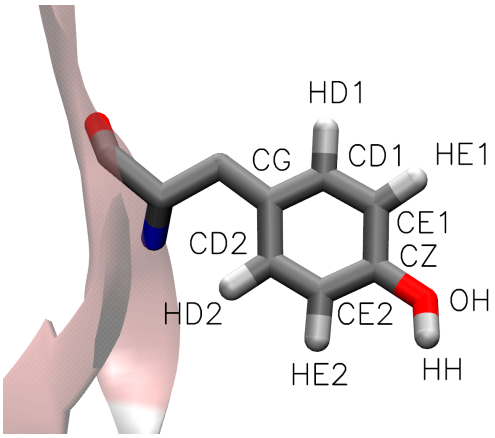

Figure 3: The phenol group of YH/Y^-/Y•, with labels matching those in Table 1.

Table 1: Partial atomic charges of the side chain of YH/Y^-/Y•. The charges for YH and Y^- are directly taken from CHARMM36.

NAME	Tyrosine (YH)	Tyrosinate (Y^-)	Radical (Y•)
HH	0.43		
OH	-0.54	-0.76	-0.205
CZ	0.11	0.40	-0.994
CE1/CE2	-0.115	-0.60	0.344
HE1/HE2	0.115	0.28	0.134
CD1/CD2	-0.115	-0.115	0.369
HD1/HD2	0.115	0.115	0.027
CG	0.00	0.00	-0.549

UV Resonance Raman Spectroscopy

The 18-mer peptides were synthesized by solid state synthesis and were obtained from Genscript USA Inc. (Piscataway, NJ) or New England Peptide (Gardner, MA). Samples were suspended in a D_2O buffer containing 5 mM sodium borate and N-cyclohexyl-3-aminopropanesulfonic acid (CAPS), pD 11, or 5 mM N-tris(hydroxymethyl)-methyl-3-aminopropanesulfonic acid (TAPS), pD 8.5, to give 1 mM solutions. The pD is reported as the uncorrected meter reading because the small solvent isotope effects on weak acid pKa values are compensated for by the D_2O-induced changes in the response of the glass electrode.[47-48] The use of D_2O buffer is necessary to observe the amide II' band, which results from uncoupling of the N-D stretch and CN stretch of the amide bond. The frequency of the amide II' band is sensitive to secondary structure.[34]

Spectra were obtained at room temperature using a 244 nm probe beam generated from an intracavity frequency-doubled argon ion laser (Cambridge LEXEL 95, Fremont, CA). The method has been described previously.[34, 49] The probe was coupled to a Raman microscope (Renishaw inVia, Hoffman Estates, IL) equipped with UV-coated, deep depletion charge-coupled device. The 1 mL sample was recirculated at a rate of 4.5 mL/min using a peristaltic pump and a focused jet to prevent UV degradation of the sample.

The radical was generated by UV photolysis with increasing power of the probe beam, described previously. The high power-minus-low power (radical-minus-singlet) difference spectrum was obtained by subtracting an averaged 340 μW from an averaged 3.4 mW scan. A total of 16 low-power scans (240 s) and 8 high-power scans (120 s) were averaged from an 8 mL sample. Previous control experiments have shown that the peptide mass is not altered by procedure. Additional details of the experimental procedures have been described previously.[34]

Results

Samples and UV resonance Raman spectroscopy. For Peptides A and C, three charge states of the tyrosine side chain were considered. In the first, predominant at pL 8.5 (where L is the lyonium ion), Y5 is in the protonated form (YH). In the second, predominant at pL 11, the Y5 side chain is anionic (Y^-). In the third, the tyrosine side chain is oxidized by one electron and deprotonated, forming a neutral radical (Y•) at both pL values

Figs. 2A and B present UVRR difference spectra, associated with oxidation of tyrosine/tyrosinate model compounds to form a neutral tyrosyl radical. The data were obtained at two different pL values in D_2O buffer. These difference spectra are associated with the generation of the radical by UV photolysis under continuous illumination.[34, 50] With UV laser probes, the vibrational spectrum of phenolic compounds is resonantly enhanced.[51] Assignments of the tyrosine, tyrosinate, and tyrosyl radical spectra have been established by previous experimental and theoretical work.[50, 52-53] Tyrosine or tyrosinate oxidation leads to spectral changes including a decrease in the frequency of the Y8a ring stretching mode and a dramatic increase in the frequency of the CO stretching mode. Positive bands reflect unique bands of the radical state; negative bands reflect unique bands of the starting, singlet YH or Y^- state. At pD 8.5 (Fig. 2A), characteristic negative bands of tyrosine at 1174, 1207, and 1610 cm^{-1} were observed; characteristic positive bands of tyrosyl radical were observed at 1408, 1516, and 1572 cm^{-1}. The spectrum at pD 11 (Fig. 2B) is similar to the spectrum acquired at pD 8.5, except for the expected shift of the Y8a ring stretching mode to 1602 cm^{-1}, due to deprotonation of the side chain.[50, 54] See Refs. [50, 52-53] for reviews of normal mode assignments.

UVRR difference spectra were also obtained from Peptides A and C at pD 8.5 (Fig. 2C, I and D, I). At this pL value, both peptides are in the YH state. The spectrum derived from Peptide A-YH (Fig. 2C, I) contains negative bands at 1441 and 1472 cm^{-1}, which are not

observed in tyrosinate or tyrosine model compound (see Fig. 2A and B). Previous work has established that these negative bands are assignable to amide II' bands.[34] These bands are negative due to a loss of Raman intensity at 244 nm in the radical state. This loss of intensity was attributed previously to a red shift of the UV electronic spectrum of the peptide backbone.[34] Such a red shift can be associated with a loss of β-strand structure,[55-56] which is driven by the YH to Y• reaction in Peptide A. Negative amide II' bands are also observed in the Peptide A-Y^- spectrum at pL 11, indicating that the putative change in structure may also occur in the Y^- to Y• reaction. However, for Peptide C (Fig. 2D, I and II), the amide II' bands are not observed at pL 11 (Y^- to Y•), although the bands are present at pL 8.5 (YH to Y•). This result implies that the YH to Y• reaction causes a conformational change in Peptide C, but that the Y^- to Y• reaction *does not* result in the same hydrogen bonding rearrangement in Peptide C.

Molecular Dynamics Simulations. We focus our analysis and presentation on β-hairpin stability and its dynamics to provide a detailed view of molecular interactions and structural information probed in the CD and UVRR experiments presented above. The conformational stability of the β-hairpin conformation of Peptide A and Peptide C and their variants was examined for three independent conventional MD simulations and one accelerated MD simulation of each system, giving a total of 7.0 μs for all simulations reported here. The Supporting Information includes the number of inter-chain backbone hydrogen bonds, radius of gyration, and distance between Y5 and residue 14 (histidine or cyclohexylalanine). The data are reported for all simulation runs on Peptide A and Peptide C in their three charge states: YH, Y^-, and Y•. Although the Y• state is extremely short-lived in vitro (picoseconds), it is maintained in the UVRR experiments for time scales exceeding those of the simulations.

Simulations of Peptide A

To describe the model's conformational dynamics, the per-residue secondary structure

assignment as a function of time was examined over the entire simulation. Fig. 4A shows that Peptide A-YH retained its β-hairpin structure, i.e., the secondary structure of residues 4-7 and 12-15 showed no change in two out of three runs. In run 3, although the Peptide A-YH lost β-sheet structure after 50 ns, it did not unfold but rather showed a propensity to recover its β-hairpin structure, preserving a long β-turn in the middle. Similarly, two out of three runs for Peptide A-Y^{-} were consistent with a stable β-hairpin conformation (see Fig. 4B).

In contrast to Peptide A-YH and A-Y^{-}, Peptide A-Y• was observed to unfold, with loss of β-hairpin structure in all three runs (see Figs. 4C and 5). However, during the first 50 ns of run 3, the peptide retained some β-bridge structure, interstrand hydrogen bonds, a stable Y5-H14 distance, and a relatively low radius of gyration. Retention of the overall fold immediately after radical generation is consistent with time-resolved absorption experiments on the 20-ps to 2-ns time scale, which have been used to study tyrosyl radical PCET in these peptides.[32-33] However, the peptide reaches the unfolded state on time scales greater than 50 ns, in agreement with the longer-time-scale UVRR experiments, supporting the experimental implication that oxidation of tyrosine results in a conformational transition from β-strand to extended form in Peptide A. Because we estimate ~3% of His14 is doubly protonated when Y5 is in a reduced state and ~25% is doubly protonated when Y5 is in a radical state (see Methods), we also simulated Peptide A-YH and Peptide A-Y• with a charged His14 for 200 ns each. Similar to their neutral His14 variants, we found Peptide A-YH to maintain its β-hairpin, while Peptide A-Y• unfolded (see Fig. S1).

Because the 200-ns simulations may not be converged, we took two alternative approaches. First, we extended one of the three runs for an additional 200 ns (400 ns total). Shown in Fig. S2, Peptide A-YH switches from a predominantly β-strand to β-turn structure after approximately 250 ns, while Peptide A-Y^{-} and Peptide A-Y• remain the same. Second, we ran 300-ns accelerated MD (aMD) simulations, in which a "boost" potential is applied to enhance

sampling of high-energy configurations.[57] The probability of the number of native hydrogen bonds was determined after reweighting the trajectories (see Fig. S4). Peptide A-YH had the highest average number of backbone hydrogen bonds (6.7 out of a possible 8), while Peptide A-Y^{-} and Peptide A-Y• had averages of 2.9 and 3.7, respectively. Although the average number of hydrogen bonds for Peptide A-Y• is apparently increased relative to Peptide A-Y^{-}, we note that the probability for more than 4 hydrogen bonds is predicted to be zero only for Peptide A-Y• (see Fig. S4). However, given that a few samples dominate the probability distribution after reweighting (see Fig. S4), a known problem[58-59], the aMD simulations are also unlikely to be converged.

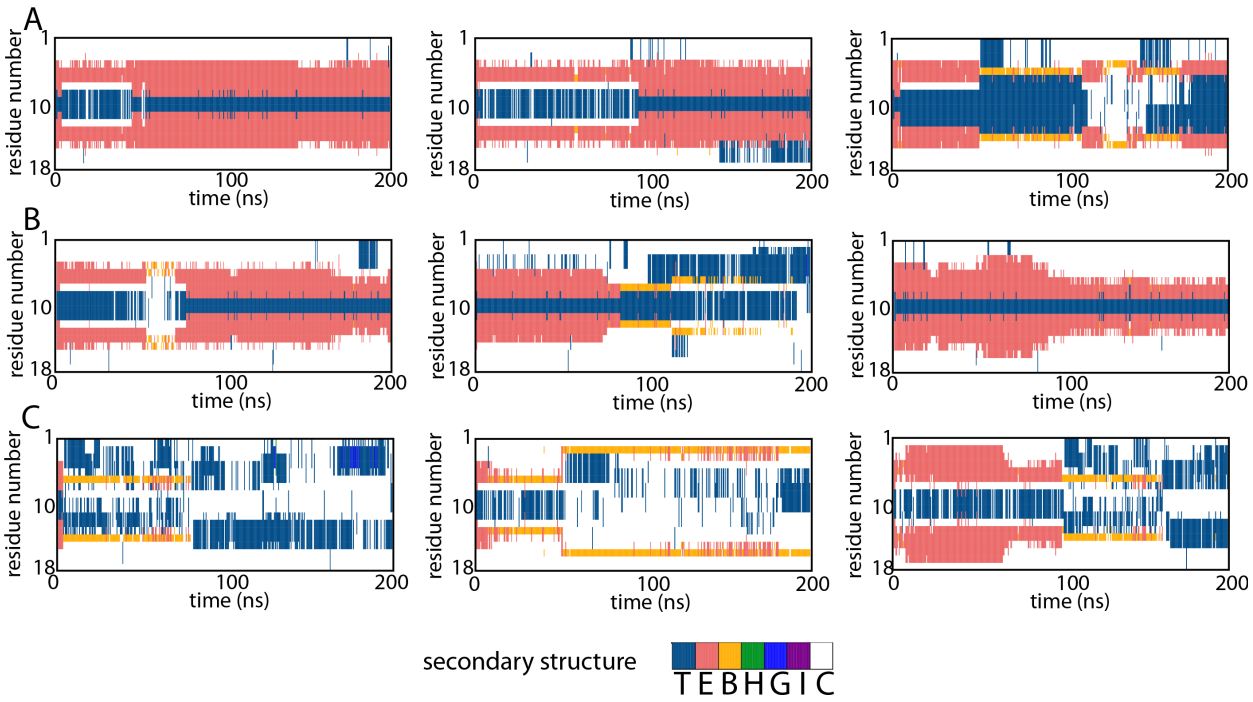

Figure 4: Time evolution of secondary-structure assignment per residue of Peptide A charge states for all three runs. Extension of the first run to 400 ns is presented in Fig. S2. The legend at the bottom uses DSSP classification as implemented in Stride[60] where T is β turn, E is β sheet, B is β bridge, H is α helix, G is 3_{10} helix, I is π helix, and C is unstructured coil. (A) Peptide A-YH. (B) Peptide A-Y^{-}. (C) Peptide A-Y•.

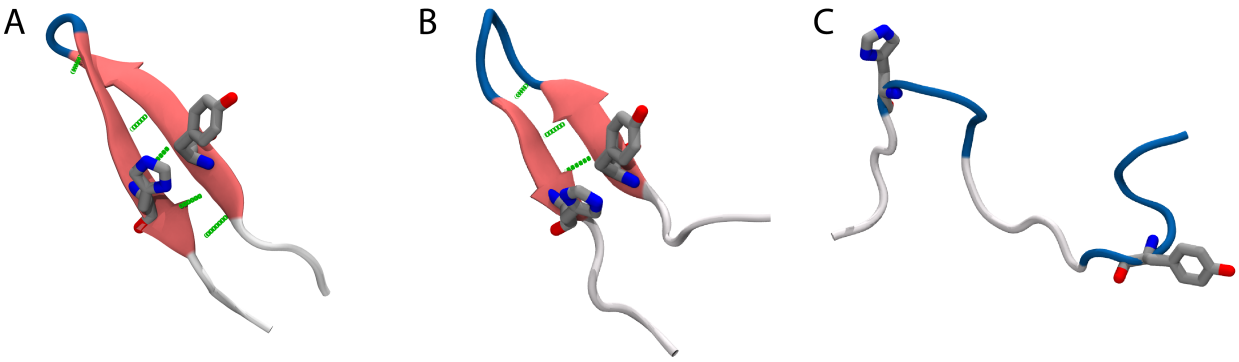

Figure 5: Examples of observed structures of (A) Peptide A-YH, (B) Peptide A-Y$^{\bullet-}$, and (C) Peptide A-Y• from run 1 of each.

Analyses of backbone hydrogen bonding support the results of the secondary structure analysis and are consistent with a redox-induced change in the Peptide A β-hairpin (See Supporting Information for analyses of all three runs). Fig. 6A shows that inter-strand hydrogen bonds are stable, enabling Peptide A-YH and Peptide A-Y$^{\bullet-}$ to remain folded in a β-hairpin conformation during their entire trajectory, while there were almost no inter-strand hydrogen bonds for Peptide A-Y• after 100 ns (see Fig. 6A, *red*). This result is further supported by analysis of the radius of gyration (R_g), which is an indicator of compactness of a protein (see Fig. 6B). Peptide A-YH and Peptide A-Y$^{\bullet-}$ remained compact, with R_g values that did not change by more than 2 Å from their native state. The folded-to-unfolded state transition of Peptide A-Y• is characterized by a significant increase in R_g (see Fig. 6B, *red*). This increase in R_g after 75 ns reflects the structural changes associated with the loss of backbone hydrogen bonding.

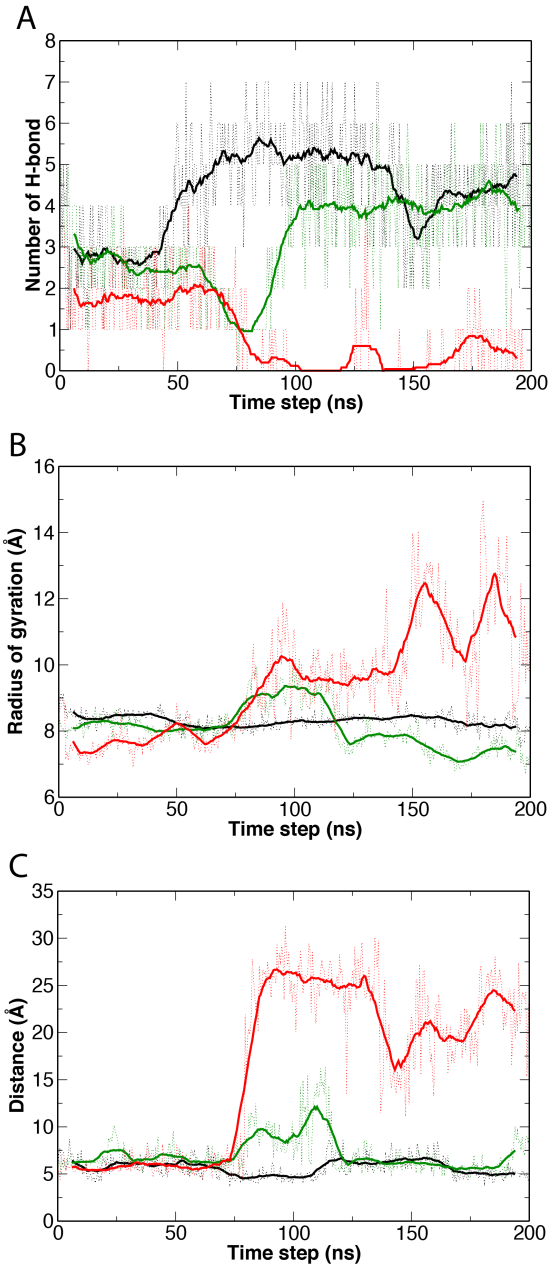

Figure 6: Structural parameters measured during simulations of Peptide A. In all panels, black curves are from run 1 of Peptide YH, green from Peptide A-Y^{-}, and red from Peptide A-Y•. Other runs are presented in Figs. S6, S7, and S8. (A) Number of backbone hydrogen bonds for each Peptide-A variant. (B) Radius of gyration. (C) Distance between Y5/Y5^{-}/Y5• and H14 of Peptide A.

We hypothesized that the stabilities of Peptide A-YH and Peptide A-$Y^{\bullet-}$ are a result of the π-π interaction between Y5/$Y5^{\bullet-}$ and H14. Consistent with this hypothesis, over most of the simulation period, the distance between Y5/$Y5^{\bullet-}$ and H14 remained within 5-10 Å (see Fig. 6C, *black/green*), due to a parallel-offset (more common) or perpendicular T-shaped (less common) stacking arrangement as seen in Fig. 7. However, the distance between these two residues for Peptide A-Y• increases to greater than 10 Å as the peptide begins to unfold, consistent with a loss of the noncovalent interaction (see Fig. 6C, *red*). Loss of this interaction is driven by unfavorable interaction energies between the two side chains; the energies for one instance of parallel-offset stacking are -0.8 kcal/mol for Peptide A-YH, -1.5 kcal/mol for Peptide A- $Y^{\bullet-}$, and +0.8 kcal/mol for Peptide A- Y• (all in identical conformations).

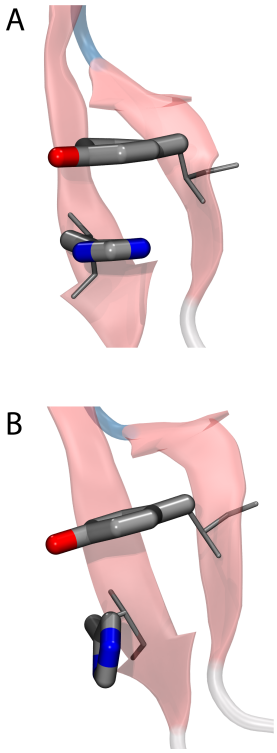

Figure 7: Arrangements for the (A) parallel offset and (B) perpendicular T-shaped π-π stacking.

Simulations of Peptide C

In Peptide C, H14 is substituted by a cyclohexylalanine (Cha14), and the π-π interaction between Y5 and the cross-strand imidazole side chain is not present. Simulations were conducted on models of Peptide C to assess its stability and to account for the pH dependence observed in the UVRR spectra. The simulations were consistent with a stable β-hairpin core in Peptide C-YH involving residues 5-8 and 11-14 (see Fig. 8A), similar to the fold observed in Peptide A-YH. Even though Peptide C-YH lost its β-hairpin conformation after 80 ns in run 2 (see Fig. 8B), the model re-attained its β-turn between residues 6-12 and a single backbone hydrogen bond between residue 2 and 17 at 150 ns. The model then formed a loop-like structure and finally recovered its β-hairpin conformation (analysis for run 2 in Supporting Information further supports this result). The stability of Peptide C-YH is also evident from analysis of its hydrogen bonds and R_g (see Fig. 9; analysis of all three runs can be found in SI). Fig. 9A shows that inter-strand hydrogen bonds in the β-hairpin formed in the initial state are maintained during in the entire 200 ns of run 1, while Fig. 9B reflects a constant R_g value.

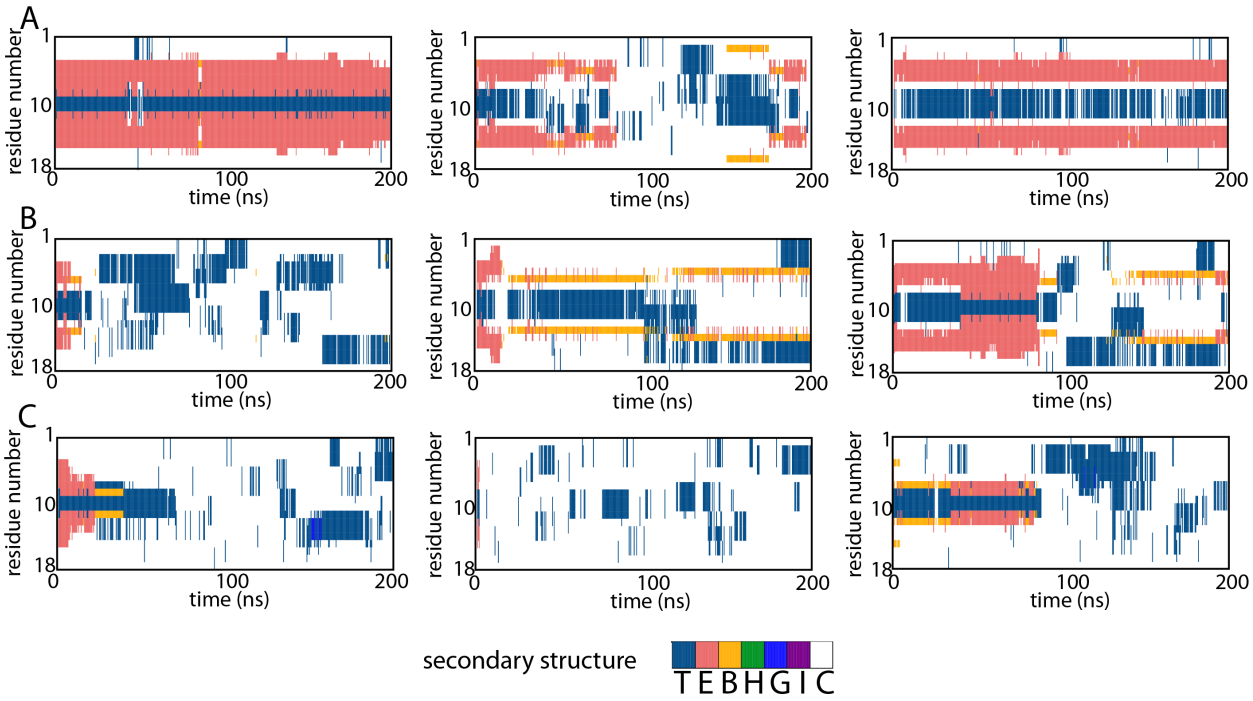

Figure 8: Time evolution of secondary-structure assignment per residue of Peptide C charge

states for all three runs. Extension of the first run to 400 ns is presented in Fig. S9. The legend at the bottom uses DSSP classification as implemented in Stride[60] where T is β turn, E is β sheet, B is β bridge, H is α helix, G is 3_{10} helix, I is π helix, and C is unstructured coil. (A) Peptide C-YH. (B) Peptide C-$Y^{\bar{-}}$. (C) Peptide C-Y•.

Peptide C-$Y^{\bar{-}}$ and Peptide C-Y• showed behaviors distinct from Peptide C-YH (see Fig. 8B and C). Unlike Peptide A-Y^{-}, which maintains its secondary structure over most of the simulations, Peptide C-Y^{-} is not as stable in a β-sheet conformation. While the Y5-Cha14 distance and radius of gyration were stable for the first few nanoseconds, large increases in both were observed by 35 ns (see Fig. 9B and C, *green*). Inter-chain hydrogen bonds were lost much more quickly, within 20 ns (see Fig. 9A, *green*). These observations suggest that the lack of π-π stacking, which is present between $Y^{\bar{-}}$ and H14 in Peptide A-Y^{-}, destabilizes the folded state of Peptide C-Y^{-}. However, two of three runs indicate that Peptide C-Y- retains a β-turn during part of the simulation (Fig. 8).

A loss of the β-hairpin conformation is evident in Peptide C-Y•. This peptide completely loses its secondary structure within 30 ns, and never comes back to a folded β-hairpin conformation. An increase in R_g and in the distance between Y5• and Cha14 (see Fig. 9B and C, *red*) also indicate that Peptide C-Y• becomes extended towards the end of the simulation. Taken together, the simulations suggest that while Peptide C-YH undergoes a hydrogen bonding change upon conversion to Peptide C-Y• at pH 8.5, Peptide C-Y^{-} does not. Singlet Peptide C-Y^{-} samples non hydrogen bonded states, and thus the structure does not change substantially when compared to Peptide C-Y•, as assessed by UVRR. These simulations provide an explanation of the pD-dependent UVRR results presented above for Peptide C. Note that CD spectra derived from Peptide C exhibited negative ellipticity at pH 5 and 11 with a

minimum wavelength similar to that of Peptide A, but with decreased amplitude. Thermal melting gave results suggesting a reversible unfolding transition in Peptide C at both pH values.[27] We attribute the previous CD results to retention of a thermostable β-turn in Peptide C in the YH and Y^- states, even though interstrand hydrogen-bonding distances have increased. Thus, we propose that while the UVRR reflects the strength of hydrogen bonding interactions, through shifts of the UV absorption band, CD reflects the presence of the β-turn,[61] which is partially retained in Peptide C-Y^-.

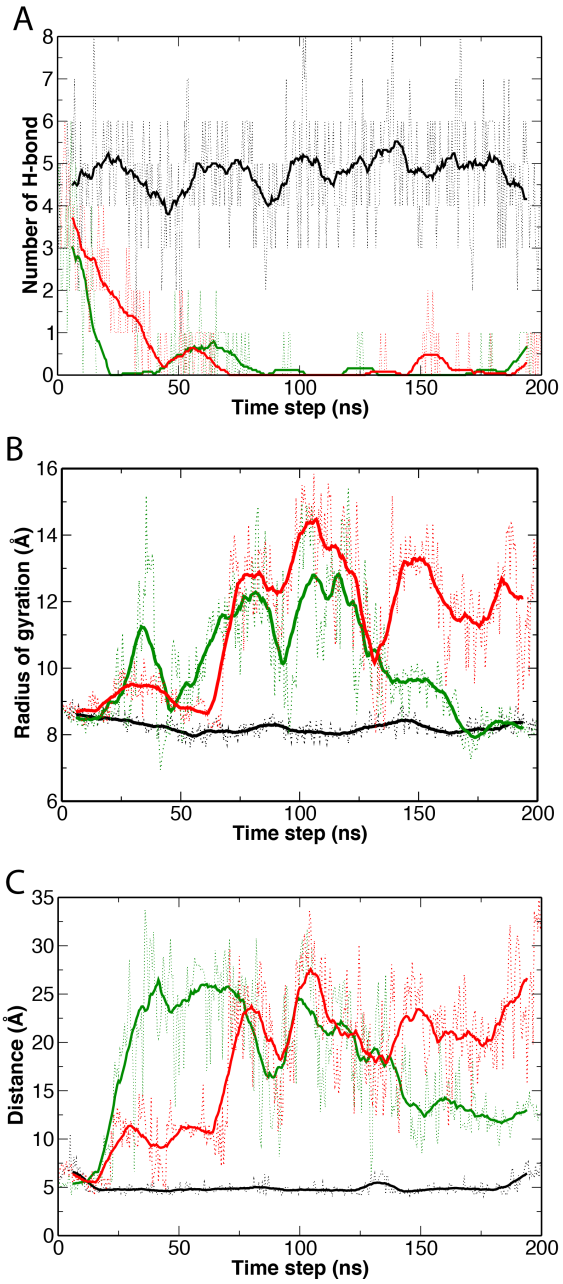

Figure 9: Structural parameters measured during simulations of Peptide C. In all panels, black curves are from run 1 of Peptide C-YH, green from Peptide C-Y^{-}, and red from Peptide C-Y•. Other runs are presented in Figs. S10, S11, and S12. (A) Number of backbone hydrogen bonds for each Peptide-C variant. (B) Radius of gyration. (C) Distance between Y5/Y5^{-}/Y5• and Cha14 of Peptide C.

We also extended one of the three runs for each Peptide-C variant to 400 ns (see Fig. S9). Peptide C-YH held its β-sheet structure for the entire simulation. Peptide C-Y^{-} gained a folded structure for the last 150 ns, while Peptide C-Y• only exhibited sporadic β-turn structure. The aMD results, given in Fig. S4, also show that Peptide C-Y^{-} and Peptide C-Y• are unstable; the average numbers of backbone-hydrogen bonds after reweighting the 300-ns aMD simulations were 3.9 (Peptide C-YH), 0 (Peptide C-Y^{-}), and 1.6 (Peptide C-Y•). Here again, we note that the probabilities tend to be dominated by a few rare events, as these high-energy states contribute the most during reweighting (see Fig. S4). [58-59]

Discussion

The design of Peptide A was inspired by two enzymes, RNR and PSII. RNR plays a pivotal role in nucleic acid metabolism and cell division,[62] and PCET reactions are important in its function.[63] In class 1a RNR, found in *E. coli* and mammals, a long-range radical transfer links the essential Y122O• in the β-subunit with the active site in the α-subunit.[64-67] Tyrosine-based radical transfer is also important in PSII, which has two redox-active tyrosines, YZ and YD, with different protein environments and different roles in electron transfer.[4, 68] EPR experiments on YD and YZ suggest that PCET distinguishes the two tyrosines.[47-48, 69] There are no structures available of the radical states. YZ and YD are oxidized on the nanosecond time scale[70], while the decay times of the radicals vary from microseconds (YZ) to hours or even days (YD) (reviewed in Ref. [71]).

Aerobic organisms require reactions such as these, which operate at high potential, but they must also protect themselves from toxic side effects. There are many unanswered questions concerning these protective mechanisms. For example, high-potential ET and PCET reactions are associated with the generation of highly reactive radical intermediates, which can irreversibly damage polypeptides. However, proteins have evolved methods to protect

themselves from this oxidative damage; one mechanism may involve radical transfer to solvent through tyrosine-tryptophan dyads.[31, 72-73] In addition, the structured protein environment is able to extend the lifetime of radical intermediates. While the lifetime of tyrosyl radicals in solution is on the microsecond time scale, in proteins, these lifetimes can be extended to hours or days. These control mechanisms are not understood, but may involve modulation of water access to the tyrosyl radical site (reviewed in Ref. [50]). Finally, proteins have devised mechanisms to trigger the tyrosyl radical to initiate an ET or PCET reaction.[61-63]

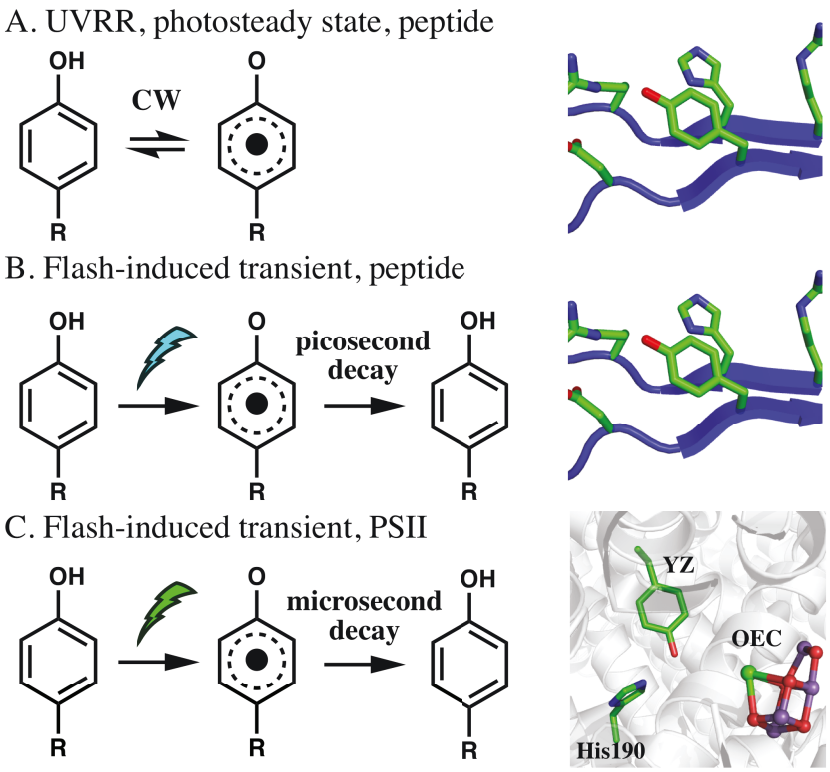

Figure 10: PCET reaction schemes for tyrosyl radical generation. (A) UVRR experiments produce a photosteady state in a peptide sample. Tyrosyl radical is generated by continuous wave (CW) illumination using 244 nm illumination and sample circulation by a peristaltic pump. Spectral subtraction (UV_{high} – UV_{low}) generates the radical-minus-singlet UVRR difference spectrum[25, 34]. (B) Time-resolved absorption spectroscopy (TRAS) generates a transient tyrosyl radical in a peptide sample. A femtosecond 280-nm pump and a stirred sample are used. The decay of radical is monitored as a transient on the picosecond time scale[25, 32-33]. (C) In PSII,

photoexcitation of chlorophyll with a visible, 532-nm pump and time-resolved absorption spectroscopy are used to measure the rate of electron transfer from tyrosine, YZ, to oxidized chlorophyll. The generation of YZ radical occurs on the nanosecond time scale and its reduction by the PSII oxygen-evolving complex (OEC) occurs on the microsecond to millisecond time scale. His190 in the D1 polypeptide is hydrogen bonded to YZ (PDB 4UB6).[70, 74-76]

In this paper, we simulated a redox-driven conformational change in a tyrosine-containing maquette, a β-hairpin peptide. Our molecular dynamics simulations provide evidence that oxidation of tyrosine in the β-hairpin maquettes, Peptide A-YH, Peptide A-Y^-, and Peptide C-YH is associated with a substantial change in secondary structure on the 100-ns time scale. In comparison to the others, Peptide C-Y^- is more dynamic, and tyrosinate oxidation in this peptide does not drive a net change in hydrogen bonding. Overall, the simulations provide evidence that the redox-driven conformational change in Peptide A is associated with a change in distance between H14 and Y5, as well as a loss of inter-strand amide hydrogen bonding. This change in distance is induced, in part, by a loss of favorable π-π stacking between H14 and Y5, due to the rearrangement of charge on the Y5 side chain in the radical state.

The kinetics of PCET have also been investigated in the β-hairpin peptides, where tyrosyl radical formation and decay occur on the picosecond time scale. In the peptides, a femtosecond UV photolysis pulse was used to generate the Peptide A- or Peptide C-Y• state, which is formed in 3 ps. The time course of radical decay was then monitored out to 2 ns (see Fig. 10B)[32-33]. The radicals decay either by recombination with the solvated electron alone (ET) or by recombination with the solvated electron and a proton (PCET), depending on the pH. This time-resolved absorption spectroscopy has shown that the decay time of the tyrosyl radical is accelerated in the β-hairpin, compared to model tyrosine or tyrosinate in solution. This effect was attributed to increased electronic coupling in the peptide.[32-33] The substitution of Cha14

(Peptide C) for H14 (Peptide A) was observed to decrease the decay rate of tyrosyl radical on this time scale at pL 9, but not at pL 11. This change shows that H14 is kinetically significant in the picosecond PCET reactions that occur at pL 9. The decrease in rate was attributed to an increase in reorganization energy in the Cha14 mutant.[33] On the time scale of these time-resolved absorption experiments, the simulated unfolding reaction is not predicted to be significant in Peptides A and C. However, in the UVRR difference experiment, which produces a photosteady state (see Fig. 10A), the predicted altered conformational state can be generated.

In photosynthetic water oxidation, a subset of the visible light-driven PCET reactions occur on the nanosecond time scale[5]. For example, the oxidation of YZ by the primary chlorophyll donor, P_{680}^{+}, is multiphasic and occurs on this time scale in active, oxygen-evolving PSII (see Fig. 10C).[70] The reduction reaction occurs on the microsecond to millisecond time scale (Figure 10C). In an ETPT or PTET mechanism, which involves rate-limiting proton transfer mechanism, or in a coupled proton electron transfer, the rate of tyrosyl radical decay would be expected to decrease as distance increases.[13, 77] Therefore, a redox-induced increase in side chain-side chain distance, as described here, could play a critical role in modulation of proton transfer rate on the hundreds of nanoseconds time scale. Note that the details of the conformational change are expected to be sequence and structure dependent. Future work will explore the impact of these factors.

Conclusions

Although not fully converged, the molecular dynamics simulations presented here provide support for the hypothesis that tyrosyl radical reactions can alter hydrogen-bonding interactions in proteins. In addition, critical distances between amino-acid side chains are shown to respond to the oxidation reaction. Such redox-coupled conformational changes may occur and be of significance in complex proteins.

Supporting Information

Description of aMD methods and results as well as 12 additional figures. The Supporting Information is available free of charge on the ACS Publications website.

The authors declare no competing financial interest.

Acknowledgment

This work was supported by NSF CLP 12-13350 (B.A.B) and NSF MCB-1452464 (J.C.G.). T.G.M. was partially supported by the Georgia Tech GAANN program in Molecular Biophysics and Biotechnology. Computational resources were provided via the Extreme Science and Engineering Discovery Environment (XSEDE), which is supported by NSF grant number OCI-1053575.

References

1. Ostermeier, C.; Harrenga, A.; Ermler, U.; Michel, H., Structure at 2.7 Å resolution of the *Paracoccus denitrificans* two-subunit cytochrome *c* oxidase complexed with an antibody FV fragment. *Proc. Natl. Acad. Sci. USA* **1997,** *94*, 10547-10553.
2. Yoshikawa, S.; Shinzawa-Itoh, K.; Nakashima, R.; Yaono, R.; Yamashita, E.; Inoue, N.; Yao, M.; Fei, M. J.; Libeu, C. P.; Mizushima, T.; et al., Redox-coupled crystal structural changes in bovine heart cytochrome c oxidase. *Science* **1998,** *280*, 1723-1729.
3. Stubbe, J., Ribonucleotide reductases: amazing and confusing. *J. Biol. Chem.* **1990,** *265*, 5329-5332.
4. Barry, B. A.; Babcock, G. T., Tyrosine radicals are involved in the photosynthetic oxygen-evolving system. *Proc. Nat. Acad. Sci. USA* **1987,** *84*, 7099-7103.
5. Pujols-Ayala, I.; Barry, B. A., Tyrosyl radicals in Photosystem II. *Biochim. Biophys. Acta* **2004,** *1655*, 205-216.
6. Kulmacz, R. J.; Ren, Y.; Tsai, A.-L.; Palmer, G., Prostaglandin H synthase: Spectroscopic studies of the interaction with hydroperoxides and with indomethacin. *Biochemistry* **1990,** *29*, 8760-8771.
7. Whittaker, M. M.; Whittaker, J. W., Tyrosine-derived free radical in apogalactose oxidase. *J. Biol. Chem.* **1990,** *265*, 9610-9613.
8. Whittaker, M. M.; Kersten, P. J.; Nakamura, N.; Sanders-Loehr, J.; Schweizer, E. S.; Whittaker, J. W., Glyoxal oxidase from *Phanerochaete chrysosporium* is a new radical-copper oxidase. *J. Biol. Chem.* **1996,** *271*, 681-687.

9. Chouchane, S.; Girotto, S.; Yu, S.; Magliozzo, R. S., Identification and characterization of tyrosyl radical formation in *Mycobacterium tuberculosis* catalase-peroxidase (KatG). *J. Biol. Chem.* **2002,** *277*, 42633-42638.
10. Huynh, M. H.; Meyer, T. J., Proton-coupled electron transfer. *Chem. Rev.* **2007,** *107*, 5004-5064.
11. Dempsey, J. L.; Winkler, J. R.; Gray, H. B., Proton-coupled electron flow in protein redox machines. *Chem. Rev.* **2010,** *110*, 7024-7039.
12. Migliore, A.; Polizzi, N. F.; Therien, M. J.; Beratan, D. N., Biochemistry and theory of proton-coupled electron transfer. *Chem. Rev.* **2014,** *114*, 3381-3465.
13. Marcus, R. A., Electron transfer reactions in chemistry: theory and experiment. *Pure & Appl. Chem.* **1997,** *69*, 13-29.
14. Edsall, J. T.; Martin, R. B.; Hollingworth, B. R., Ionization of individual groups in dibasic acids, with application to the amino and hydroxyl groups of tyrosine. *Proc. Natl. Acad. Sci. USA* **1958,** *44*, 505-519.
15. Dixon, W. T.; Murphy, D., Determination of the acidity constants of some phenol radical cations by means of electron spin resonance. *J. Chem. Soc. London, Faraday Trans. II* **1976,** *72*, 1221-1230.
16. Barry, B. A.; El-Deeb, M. K.; Sandusky, P. O.; Babcock, G. T., Tyrosine radicals in photosystem II and related model compounds. *J. Biol. Chem.* **1990,** *265*, 20139-20143.
17. Hammes-Schiffer, S.; Soudackov, A. V., Proton-coupled electron transfer in solution, proteins, and electrochemistry. *J. Phys. Chem. B* **2008,** *112*, 14108-14123.
18. Jones II, G.; Vullev, V.; Braswell, E. H.; Zhu, D., Multistep photoinduced electron transfer in a *de novo* helix bundle: multimer self-assembly of peptide chains including a chromophore special pair. *J. Am. Chem. Soc.* **2000,** *122*, 388-389.
19. Lombardi, A.; Nastri, F.; Pavone, V., Peptide-based heme-protein models. *Chem. Rev.* **2001,** *101*, 3165-3190.
20. Gibney, B. R.; Huang, S. S.; Skalicky, J. J.; Fuentes, E. J.; Wand, A. J.; Dutton, P. L., Hydrophobic modulation of heme properties in heme protein maquettes. *Biochemistry* **2001,** *40*, 10550-10561.
21. Discher, B. M.; Noy, D.; Strzalka, J.; Ye, S.; Moser, C. C.; Lear, J. D.; Blasie, J. K.; Dutton, P. L., Design of amphiphilic protein maquettes: Controlling assembly, membrane insertion, and cofactor interactions. *Biochemistry* **2005,** *44*, 12329-12343.
22. Cochran, F. V.; Wu, S. P.; Wang, W.; Nanda, V.; Saven, J. G.; Therien, M. J.; DeGrado, W. F., Computational *de novo* design and characterization of a four-helix bundle protein that selectively binds a nonbiological cofactor. *J. Am. Chem. Soc.* **2005,** *127*, 1346-1347.
23. Tommos, C.; Skalicky, J.; Pilloud, D. L.; Wand, A. J.; Dutton, L. P., De novo proteins as models of radical enzymes. *Biochemistry* **1999,** *38*, 9495-9507.
24. Di Bilio, A. J.; Crane, B. R.; Wehbi, W. A.; Kiser, C. N.; Abu-Omar, M. M.; Carlos, R. M.; Richards, J. H.; Winkler, J. R.; Gray, H. B., Properties of photogenerated tryptophan and tyrosyl radicals in structurally characterized proteins containing rhenium(I) tricarbonyl diimines. *J. Am. Chem. Soc.* **2001,** *123*, 3181-3182.
25. Sibert, R. S.; Josowicz, M.; Porcelli, F.; Veglia, G.; Range, K.; Barry, B. A., Proton-coupled electron transfer in biomimetic peptide as a model of enzyme regulatory mechanism. *J. Am. Chem. Soc.* **2007,** *129*, 4393-4400.

26. Li, S.; Su, Y.; Luo, W.; Hong, M., Water-protein interactions of an arginine-rich membrane peptide in lipid bilayers investigated by solid-state nuclear magnetic resonance spectroscopy. *J. Phys. Chem. B* **2010,** *114*, 4063-4069.
27. Sibert, R. S.; Josowicz, M.; Barry, B. A., Control of proton and electron transfer in *de novo* designed, biomimetic β hairpins. *ACS Chem. Biol.* **2010,** *5*, 1157-1168.
28. Martinez-Rivera, M. C.; Berry, B. W.; Valentine, K. G.; Westerlund, K.; Hay, S.; Tommos, C., Electrochemical and structural properties of a protein system designed to generate tyrosine Pourbaix diagrams *J. Am. Chem. Soc.* **2011,** *133*, 17786-17795
29. Ravichandran, K. R.; Liang, L.; Stubbe, J.; Tommos, C., Formal reduction potential of 3,5-difluorotyrosine in a structured protein: insight into multistep radical transfer. *Biochemistry* **2013,** *52*, 8907-8915.
30. Glover, S. D.; Jorge, C.; Liang, L.; Valentine, K. G.; Hammarstrom, L.; Tommos, C., Photochemical tyrosine oxidation in the structurally well-defined alpha3Y protein: proton-coupled electron transfer and a long-lived tyrosine radical. *J. Am. Chem. Soc.* **2014,** *136*, 14039-14051.
31. Pagba, C. V.; McCaslin, T. G.; Veglia, G.; Porcelli, F.; Yohannan, J.; Guo, Z.; McDaniel, M.; Barry, B. A., A tyrosine-tryptophan dyad and radical-based charge transfer in a ribonucleotide reductase-inspired maquette. *Nat. Commun.* **2015,** *6*, 10010.
32. Pagba, C. V.; Chi, S. H.; Perry, J.; Barry, B. A., Proton-coupled electron transfer in tyrosine and a beta-hairpin maquette: reaction dynamics on the picosecond time scale. *J. Phys. Chem. B* **2015,** *119*, 2726-2736.
33. Pagba, C. V.; McCaslin, T. G.; Chi, S. H.; Perry, J. W.; Barry, B. A., Proton-Coupled Electron Transfer and a Tyrosine-Histidine Pair in a Photosystem II-Inspired beta-Hairpin Maquette: Kinetics on the Picosecond Time Scale. *J. Phys. Chem. B* **2016,** *120*, 1259-1272.
34. Pagba, C. V.; Barry, B. A., Redox-induced conformational switching in photosystem-II-inspired biomimetic peptides: a UV resonance Raman study. *J. Phys. Chem. B* **2012,** *116*, 10590-10599.
35. Bixon, M.; Jortner, J., Coupling of protein modes to electron transfer in bacterial photosynthesis. *J. Phys. Chem.* **1986,** *90*, 3795–3800.
36. Moser, C. C.; Keske, J. M.; Warncke, K.; Farid, R. S.; Dutton, P. L., Nature of biological electron transfer. *Nature* **1992,** *355*, 796-802.
37. Mayer, J. M., Proton-coupled electron transfer: a reaction chemist's view. *Ann. Rev. Phys. Chem.* **2004,** *55*, 363-390.
38. Cukier, R. I., Theory and simulation of proton-coupled electron transfer, hydrogen atom transfer, and proton translocation in proteins. *Biochimica et Biophysica Acta* **2004,** *1655*, 37-44.
39. Mayne, C. G.; Saam, J.; Schulten, K.; Tajkhorshid, E.; Gumbart, J. C., Rapid parameterization of small molecules using the Force Field Toolkit. *J. Comput. Chem.* **2013,** *34*, 2757-2770.
40. Humphrey, W.; Dalke, A.; Schulten, K., VMD – Visual Molecular Dynamics. *J. Mol. Graphics* **1996,** *14*, 33-38.
41. Vanommeslaeghe, K.; Hatcher, E.; Acharya, C.; Kundu, S.; Zhong, S.; Shim, J.; Darian, E.; Guvench, O.; Lopes, P.; Vorobyov, I.; et al., CHARMM general force field: A force field for drug-like molecules compatible with the CHARMM all-atom additive biological force fields. *J. Comput. Chem.* **2010,** *31*, 671-690.

42. Bally, T.; Borden, W. T., Calculations on Open-Shell Molecules: A Beginner's Guide. In *Reviews in Computational Chemistry*, John Wiley & Sons, Inc.: 2007; pp 1-97.
43. Frisch, M. J.; Trucks, G. W.; Schlegel, H. B.; Scuseria, G. E.; Robb, M. A.; Cheeseman, J. R.; Scalmani, G.; Barone, V.; Mennucci, B.; Petersson, G. A.; et al., *Gaussian 09, Revision D.01*. Gaussian, Inc., Wallingford CT: 2009.
44. Phillips, J. C.; Braun, R.; Wang, W.; Gumbart, J.; Tajkhorshid, E.; Villa, E.; Chipot, C.; D. Skeel, R.; Kale, L.; Schulten, K., Scalable molecular dynamics with NAMD. *J. Comput. Chem.* **2005,** *26*, 1781-1802.
45. Best, R. B.; Zhu, X.; Shim, J.; Lopes, P. E.; Mittal, J.; Feig, M.; MacKerell Jr., A. D., Optimization of the additive CHARMM all-atom protein force field targeting improved sampling of the backbone φ, ψ and side-chain χ1 and χ2 dihedral angles. *J. Chem. Theor. Comput.* **2012,** *8*, 3257-3273.
46. Darden, T. A.; York, D. M.; Pedersen, L. G., Particle mesh Ewald: An N log N method for Ewald sums in large systems. *J. Comput. Phys.* **1993,** *98*, 10089-10092.
47. Jenson, D.; Evans, A.; Barry, B. A., Proton-coupled electron transfer and tyrosine D of photosystem II. *J. Phys. Chem. B* **2007,** *111*, 12599-12604.
48. Jenson, D. L.; Barry, B. A., Proton-coupled electron transfer in Photosystem II: Proton inventory of a redox active tyrosine. *J. Am. Chem. Soc.* **2009,** *131*, 10567-10573.
49. Chen, J.; Barry, B., Ultraviolet resonance Raman microprobe spectroscopy of photosystem II. *Photochem. Photobiol.* **2008,** *84*, 815-818.
50. Barry, B. A.; Chen, J.; Keough, J.; Jenson, D. L.; Offenbacher, A. R.; Pagba, C. V., Proton coupled electron transfer and redox active tyrosines: Structure and function of the tyrosyl radicals in ribonucleotide reductase and photosystem II. *J. Phys. Chem. Lett.* **2012,** *3*, 543-554.
51. Asher, S. A., UV resonance Raman spectroscopy for analytical, physical, and biophysical chemistry. *Anal. Chem.* **1993,** *65*, A59-A66.
52. Johnson, C. R.; Ludwig, M.; Asher, S. A., Ultraviolet resonance Raman characterization of photochemical transients of phenol, tyrosine, and tryptophan. *J. Am. Chem. Soc.* **1986,** *108*, 905-912.
53. Range, K.; Ayala, I.; York, D.; Barry, B. A., Normal modes of redox-active tyrosine: conformation dependence and comparison to experiment. *J. Phys. Chem. B* **2006,** *110*, 10970-10981.
54. Barry, B. A., Reaction dynamics and proton coupled electron transfer: studies of tyrosine-based charge transfer in natural and biomimetic systems. *Biochim. Biophys. Acta* **2015,** *1847*, 46-54.
55. Rosenheck, K.; Doty, P. T., The far ultraviolet absorption spectrum of polypeptide and protein solutoins and their dependence on conformation. *Proc. Natl. Acad. Sci. USA* **1961,** *47*, 1775-1785.
56. Copeland, R. A.; Spiro, T. G., Secondary structure determination in proteins from deep (192-223-nm) ultraviolet Raman spectroscopy. *Biochemistry* **1987,** *26*, 2134-9.
57. Hamelberg, D.; Mongan, J.; McCammon, J. A., Accelerated molecular dynamics: a promising and efficient simulation method for biomolecules. *J. Chem. Phys.* **2004,** *120*, 11919-11929.
58. Shen, T.; Hamelberg, D., A statistical analysis of the precision of reweighting-based simulations. *J. Chem. Phys.* **2008,** *129*, 034103.

59. Sinko, W.; Miao, Y.; de Oliveira, C. A. F.; McCammon, J. A., Population Based Reweighting of Scaled Molecular Dynamics. *J. Phys. Chem. B* **2013,** *117*, 12759-12768.
60. Frishman, D.; Argos, P., Knowledge-based protein secondary structure assignment *Proteins: Struct., Funct., Genet.* **1995,** *23*, 566-579.
61. Kawai, M.; Fasman, G., A model β turn. Circular dichroism and infrared spectra of a tetrapeptide. *J. Am. Chem. Soc.* **1978,** *100*, 3630-3632.
62. Jordan, A.; Reichard, P., Ribonucleotide reductases. *Ann. Rev. Biochem.* **1998,** *67*, 71-98.
63. Minnihan, E. C.; Nocera, D. G.; Stubbe, J., Reversible, long-range radical transfer in *E. coli* class Ia ribonucleotide reductase. *Acc. Chem. Res.* **2013,** *46*, 2524-2535.
64. Högbom, M.; Galander, M.; Andersson, M.; Kolberg, M.; Hofbauer, W.; Lassmann, G.; Nordlund, P.; Lendzlan, F., Displacement of the tryosyl radical cofactor in ribonucleotide reductase obtained by single-crystal high-field EPR and 1.4-A X-ray data. *Proc. Nat. Acad. Sci. USA* **2003,** *100*, 3209-3214.
65. Offenbacher, A. R.; Vassiliev, I. R.; Seyedsayamdost, M. R.; Stubbe, J.; Barry, B. A., Redox-linked structural changes in ribonucleotide reductase. *J. Am. Chem. Soc.* **2009,** *131*, 7496-7497.
66. Offenbacher, A. R.; Burns, L. A.; Sherrill, C. D.; Barry, B. A., Redox-linked conformational control of proton-coupled electron transfer: Y122 in the ribonucleotide reductase beta2 subunit. *J. Phys. Chem. B* **2013,** *117*, 8457-8468.
67. Kasanmascheff, M.; Lee, W.; Nick, T. U.; Stubbe, J.; Bennati, M., Radical transfer in E. coli ribonucleotide reductase: a NH2Y731/R411A-α mutant unmasks a new conformation of the pathway residue 731. *Chem. Sci.* **2016,** *7*, 2170-2178
68. Boerner, R. J.; Barry, B. A., Isotopic labeling and EPR spectroscopy show that a tyrosine residue is the terminal electron donor, Z, in manganese-depleted photosystem II preparations. *J. Biol. Chem.* **1993,** *268*, 17151-17154.
69. Keough, J.; Jenson, D. L.; Zuniga, A.; Barry, B. A., Proton coupled electron transfer and redox-active tyrosine Z in the photosynthetic oxygen evolving complex. *J. Am. Chem. Soc.* **2011,** *133*, 11084-11087.
70. Renger, G., Oxidative photosynthetic water splitting: energetics, kinetics and mechanism. *Photosynth. Res.* **2007,** *92*, 407-425.
71. Barry, B. A., Proton coupled electron transfer and redox active tyrosines in photosystem II. *J. Photochem. Photobiol. B* **2011,** *104*, 60-71.
72. Winkler, J. R.; Gray, H. B., Could tyrosine and tryptophan serve multiple roles in biological redox processes? *Philos. Trans. A Math. Phys. Eng. Sci.* **2015,** *373*.
73. Gray, H. B.; Winkler, J. R., Hole hopping through tyrosine/tryptophan chains protects proteins from oxidative damage. *Proc. Natl. Acad. Sci. USA* **2015,** *112*, 10920-10925.
74. Ahlbrink, R.; Haumann, M.; Cherepanov, D.; Bogershausen, O.; Mulkidjanian, A.; Junge, W., Function of tyrosine Z in water oxidation by photosystem II: Electrostatical potential instead of hydrogen abstractor. *Biochemistry* **1998,** *37*, 1131-1142.
75. Umena, Y.; Kawakami, K.; Shen, J.-R.; Kamiya, N., Crystal structure of oxygen-evolving photosystem II at a resolution of 1.9 Å ngstrom. *Nature* **2011,** *473*, 55-60.

76. Suga, M.; Akita, F.; Hirata, K.; Ueno, G.; Murakami, H.; Nakajima, Y.; Shimizu, T.; Yamashita, K.; Yamamoto, M.; Ago, H.; et al., Native structure of photosystem II at 1.95 Å resolution viewed by femtosecond X-ray pulses. *Nature* **2015,** *517*, 99-103.
77. Mayer, J. M., A simple Marcus-theory type model for hydrogen atom transfer/proton-coupled electron transfer. *J. Phys. Chem. Lett.* **2011,** *2*, 1481-1489.

TOC graphic